# Hyperthermic Application of Manganese Doped Cobalt Ferrite Nanoparticles in Therapeutic Treatment of Cancer

*Ahsan MZ[1,2,3],\* Kamal MM[2], Rakhi SS[2], Tanha SN[2], Hasan GI[2], Ahmed MJ[2], Ahmed T[2], Roxana Ferdousi Era[2]*

[1]Department of Physics, Bangladesh University of Engineering and Technology, Dhaka, Bangladesh

[2]Departments of Chemistry and Physics, Gono Bishwabidyalay, Savar, Dhaka, Bangladesh

[3]Military Institute of Science and Technology, Mirpur Cantonment, Dhaka-1216, Bangladesh

## *Corresponding author:

**Dr. Md. Ziaul Ahsan**

Military Institute of Science and Technology, Mirpur Cantonment, Dhaka-1216, Bangladesh, Phone: 01769760880; Email: ziaul8808828@gmail.com

## ABSTRACT

The results on the dynamic response of magnetic behavior, associated with the mechanism of producing heat, of manganese doped cobalt ferrite nanoparticles with the composition formula $Co_{1-x}Mn_xFe_2O_4$ ($0.125 \leq x \leq 0.5$) are reported in this research article to highlight its potential medical related applications, in particular hyperthermic application in therapeutic approach for tumor cancer treatment. The samples were prepared through the solid-state reaction route using the ball milling technique. The X-ray diffraction profile demonstrates a rising trend in crystallite size (64.02nm – 67.17nm) with the Mn content. The non-responsive of the imaginary part of complex permeability with increasing frequency represents a constant conversion of electromagnetic energy into heat. The magnetic modulus analysis examined the correlation between structural/microstructural and magnetic relaxation loss. The peaks in the spectrum of the imaginary part correspond to the resonance frequency that follows the increasing trend of crystallite size with increasing Mn content and entails the absorption of magnetic energy from the alternating magnetic field that heats the material, produced by the mechanism of magnetic relaxation loss. Thus, this heating energy becomes tunable with the Mn content and marks the sample suitable to be used in magnetic induction hyperthermia therapeutic treatment of breast cancer as well as other tumor cancer after optimizing the required temperature and functionalizing with the necessary biocompatible materials, which is alleged as its novelty of this study because of fostering this relaxation magnetic loss as an alternative use in medical fields.

**Keywords:** Manganese dopped Cobalt ferrite, Permeability, Magnetic modulus, Hyperthermia

## INTRODUCTION

Worldwide cancers have become major concern to the scientist

community. As such, study is continuing globally to explore suitable material for the treatment of tumor cancers, particularly in the breast and beneath the skin using magnetic induction hyperthermia (MIH). This MIH is an oncological therapeutic approach to treat tumor cancers used simultaneously with other therapies like chemotherapy, radiation therapy and so on. Iron oxide magnetic nanoparticles (MNPs) are extensively used in MIH. Marta Vassallo, et al. reported that in MIH, the said nano particles are injected in the body and carried through the blood circulatory system to the cancer infected area. Then, these particles are activated by alternating current (AC) magnetic field that release heat through hysteresis loss at temperature around 470C to kill cancer cells without destroying healthy cells [1]. Yu, X., Yang, R., Wu, C. et al reported that the heating efficiency of MNPs converting electromagnetic energy to thermal energy is decisive by the performance of MNPs in MIH. This performance of MNPs to produce higher heating efficiency depends mostly on the particle size and magnetic state. Hysteresis loss and relaxation loss are the two major mechanisms of producing heating energy in the MNPs under the influence of AC magnetic field [2]. A. S. Garanina et al. reported that "cobalt ferrite magnetic nanoparticles (MNPs) demonstrate a perspective platform for tumor therapy by MIH due to the ability of producing effective heating without exerting a toxic effect on the organism" [3]. M. Z. Ahsan et al also reported that non-stoichiometric composition $Co_{1+x}Mn_xFe_{2-x}O_4$ of manganese doped cobalt ferrite nanoparticles may be a suitable candidate to be used in hyperthermic treatment by released heat due to eddy current loss [4]. The objective of this research article is to explore the possibility of using manganese doped cobalt ferrite nanoparticles with the composition formula $Co_{1-x}Mn_xFe_2O_4$ in MIH by releasing heating energy through the mechanism of magnetic relaxation loss. In this study, the samples were prepared by conventional solid state reaction route and characterized for the structural properties by XRD and the complex permeability using impedance analyzer over the frequency band 100Hz to 10MHz for the analysis of magnetic "modulus. The complex permeability refers to the dynamic response of magnetic behavior by the alternating magnetic field and is described by the relation, $\mu = \mu' - j\mu''$ where $\mu'$ represents the real part and $\mu''$ imaginary part" [5]. The phase between the response of magnetic domains and applied field determines its real and imaginary parts. The function frequency ascertains the dynamic condition of the magnetic domains, which is associated with the mechanism of hysteresis and relaxation losses. The relaxation loss is correlated to the microstructure. The magnetic modulus, determined from the measurement of the complex permeability by usual formulism [5,6], is an important tool that has been examined for understanding the relaxation loss associated with the structural correlation of the investigated samples by separating the local behavior of defects from the effects of air gap, stray effect, and so on [6]. The XRD profile shows the increasing trend of crystallite size with manganese content. The peak in the spectrum of the imaginary part ($M''_m$) of magnetic modulus corresponds to the resonance frequency $f_{resonance}$ [5-8]. This resonance frequency is found to follow the increasing trend of crystallite size with increasing Mn content and is associated the magnetic relaxation loss by the relation $\tau_m = 1/2\pi f_{resonance}$ [5,6] and $\tan \delta = M''/M' = \omega\tau_m$ that produces the heating energy under the influence of alternating current (AC) magnetic field [9-13]. Thus, this heating energy turns out to be tunable with the Mn content. This tunable heating energy may make the sample suitable to be used in MIH for therapeutic treatment of breast cancer and cancer beneath the skin after optimizing the required temperature in the range $42^0C$–$47^0C$ and functionalizing with the biocompatible materials. The option of using this relaxation loss in MIH may be alleged as a novelty of this study.

## EXPERIMENTAL DETAILS

### Synthesis Method

The investigated samples were prepared by the conventional solid state reaction method with the composition formula $Co_{1-x}Mn_xFe_2O_4$ (x = 0.125, 0.25, 0.375 and 0.5). In that, the laboratory graded powders of $Co_2O_3$, $MnO_2$, and $Fe_2O_3$ with purity around 97% were mixed in desired proportion and grinded by hand in a mortar with pestle for 2 h. The mixed powders of samples were ball milled for 10 h by using the planetary ball milling technique (MSK-SFM-1benchtop) and then calcined at 900 °C in the WiseTherm furnace for 1 h. The toroid samples were then prepared by the handmade hydraulic pressing machine using dice of proper geometry at a pressure of 5000 psi (pound per square inch). The toroid of investigated samples was then sintered at $1050^0$ C in the same furnace for 1 h [6,14-17]. Thus, samples were made ready for characterization. The pictorial flow chart [6] is shown in the following Figure 1 for better understanding.
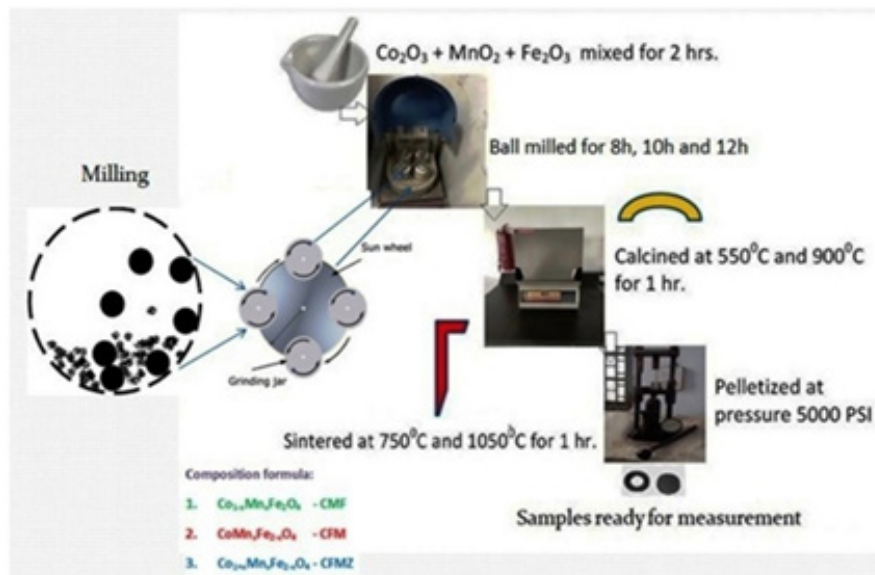
**Figure 1.** Pictorial flow chart of sample preparation method by solid-state reaction route using ball milling [6].

## Characterization

The calcined powders of the samples were used to examine the structural characteristics by using the X-ray diffractometer (EMPYREAN PANalytical) [10]. The XRD profile is shown in Figure 1(a). The field emission electron microscopic (FESEM, JEOL model JSM-7600F) images as shown ion Figure 1(b) were used to study the morphological characteristics of the samples. Image J soft was employed to scale the particle size using line method the complex permeability was measured by the Waynekerr Impedance Analyzer 6500B using toroid shape sampis over the frequency band 100 Hz–10 MHz at room temperature. Their magnetic modulus was then computed from the values of real and imaginary parts of complex permeability using the usual modulus formalism as reported in the literature [6,14-17].

## RESULT AND DISCUSSION

### Structural properties

Figure 2 (a) shows the XRD profile of the $Co_{1-x}Mn_xFe_2O_4$. The observed peaks at Miller indices (111), (220), (311), (400), (422) and (511) are found well matched with the standards JCPDS card No. 22-1086 for $CoFe_2O_4$ and indicate the single-phase cubic spinel structure [6, 16-20]. The crystallinity of the investigated samples is confirmed by the intense sharp peaks has seen in the XRD profile. The X'pertpro High Score Plus software used to determine peak position (2 ) and full width at half maximum (FWHM) of the strongest peak that matched to the Miller plane (311) and also used to compute the lattice constant (a) and the crystallite size (Dx) by using the usual formulas [5,6]. The hopping and bond lengths were calculated by using Stanley's equations [6,14-17]. Figure-2 (b) shows the FE-SEM micrographs for the samples of different Mn content (x = 0.125, 0.25, 0.375 0.5). All these structural parameters are listed in the following Table-1:
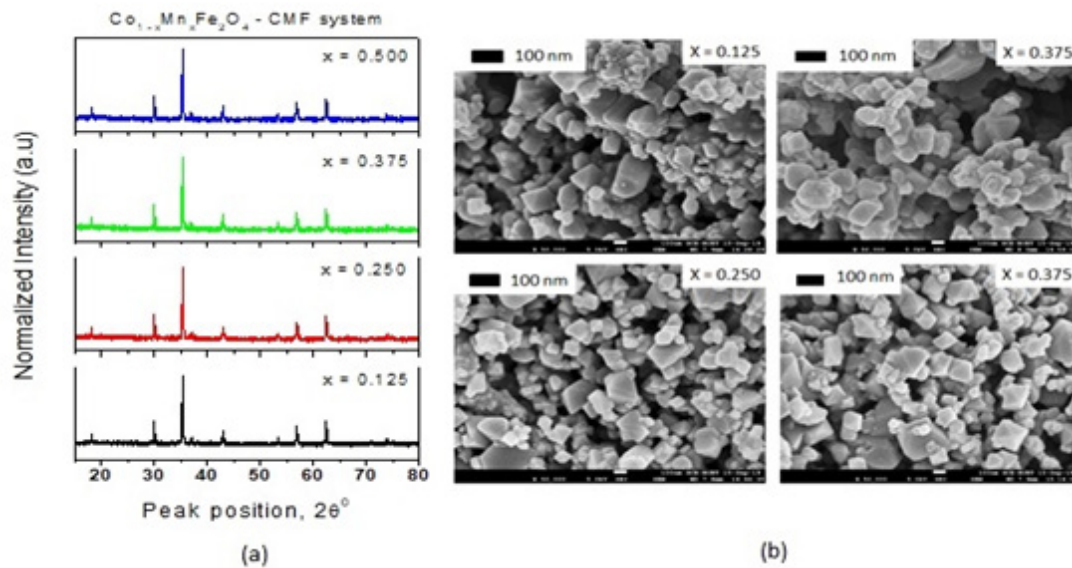
**Figure 2.** (a) X-ray diffraction patterns (b) FE-SEM Micrographs for samples of the CMF system with Mn content (x) = 0.125, 0.25, 0.375 and 0.5.

**Table 1.** Structural parameters of $Co_{1-x}Mn_xFe_2O_4$ as determined from the XRD profile

| Mn(x) | 2θ of (311) plane | FWHM | $a$(Å) | $D_x$ (nm) | $L_A$(Å) | $L_B$(Å) | A-O(Å) | B-O(Å) | Particle Size (PS) (nm) |
|---|---|---|---|---|---|---|---|---|---|
| 0.125 | 35.515 | 0.1304 | 8.383 | 64.02 | 3.630 | 2.964 | 1.817 | 2.097 | 32 |
| 0.250 | 35.521 | 0.1248 | 8.382 | 66.90 | 3.629 | 2.963 | 1.815 | 2.095 | 30 |
| 0.375 | 35.525 | 0.1245 | 8.381 | 67.10 | 3.627 | 2.962 | 1.813 | 2.092 | 28 |
| 0.500 | 35.531 | 0.1243 | 8.380 | 67.17 | 3.623 | 2.960 | 1.811 | 2.089 | 24 |

Table-1 shows that the crystallite size (Dx) increases with Mn content that may be triggered by the effect of smaller scale of dopant (Mn) ion [6]. However, a slight decrease in lattice constant (a), hopping lengths and bond lengths is marked with increasing Mn content (x) as reported in literatures [6,15]. The FE-SEM micrographs, as seen in Figure 1(b), demonstrate uneven and non-spherical shapes of particles that leading to randomly agglomeration. The line method using the Image-J software employed to estimate average particle size and presented in Table 1. The average particle sizes are found to follow the decreasing trend of lattice constant due to relatively smaller ionic size of Mn2+[5,6,14].
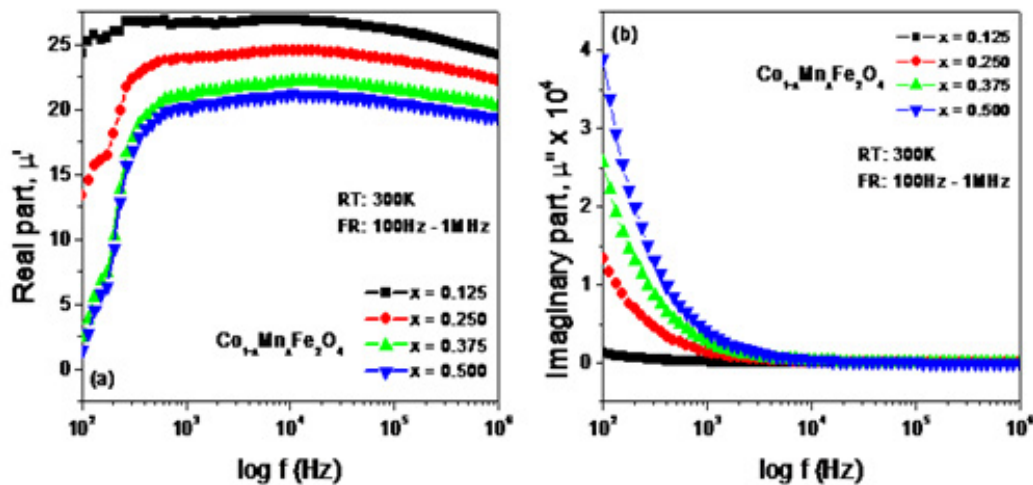
**Complex Permeability**



**Figure 3.** (a) Real part, $\mu'$ (b) Imaginary part, $\mu''$ for the sample of Co1-xMnxFe2O4 at different Mn(x) in the frequency range 100Hz – 1MHz.

Figure 3(a) shows the dispersion of $\mu'$ for the investigated samples (toroid shaped) of Co1-xMnxFe2-xO4 at room temperature (RT). "The initial rise in $\mu'$ with the applied frequency up to around 550Hz may cause from the collective effect of the domain wall motions and spin rotations. A very slight linear decrease in $\mu'$ with the applied frequency seems to be almost constant over the band 550Hz–1MHz" [5]. This behavior of $\mu'$ may be attributed to the damping mechanism of spin only rotations due to nanosized particles [5,6,15]. "Over the whole frequency band (100Hz–1MHz) the magnitude of $\mu'$ decreases with the increase in Mn content (x) due to the antiferromagnetic effect of Mn2+.in the B site. Figure 3 (b) shows the dispersion of $\mu''$ for the same samples. An almost exponential decrease in $\mu''$ up to around 1.5 kHz is observed in its dispersion that may be due to the damping mechanism of dipolar orientations" [6]. Afterward, $\mu''$ becomes non-responsive to the applied frequency over the band 1.5 kHz –1MHz and is expected to cause from the spin only rotations due to their nanosized particles [5,6,15]. This non-responsive or independence in behavior of $\mu''$ over the above frequency band (1.5 kHz –1MHz) symbolizes the conversion of electromagnetic energy into a constant heating energy that may mark this material a suitable candidate to be used in medical related devices where low and constant temperature is required.

**Magnetic Modulus**

Figure 4 shows the spectrum of the real part *M'm* and the

imaginary part *M''m* of the magnetic modules. As seen in Figure 4(a), an almost exponential increase of *M'm* is observed with increasing applied frequency. This frequency responsiveness may be attributed to the combined effect of dipolar (wall relaxation) and spin rotations (rotational resonance) in the magnetization process and associated with the magnetic relaxation loss in the solid according to Neel's relaxation [5,6,10]. Following that, *M'm* is observed to have a small linear increase to a single asymptotic value that entailing the domination of spin rotations (rotational resonance) only [5,6,19-21]. Figure 4(b) shows the increasing and decreasing trend up to and from well-resolved peaks in the dispersion of *M''m* with increasing applied frequency. A rightward shifting of the peaks with Mn content is also noticed in the spectrum that involves more damping of wall motion compared to that of the spin rotations owing to hindrances offered by pinning sites originated from oxygen vacancies that triggering absorption of magnetic energies [4-6]. The frequency corresponds to the peak is known as the resonance frequency $f_{resonance}$ that is associated with the magnetic relaxation loss and follows the increasing trend of the crystallite size as shown in the Table-1. This increasing fact demonstrates that the resonance frequency $f_{resonance}$ is directly related to their crystallite size [5,6,9,14,15]. The relaxation time constant $\tau_m$ determines this magnetic relaxation loss tan δ, given by the relation, tan $\delta = M''/M' = \omega\tau_m$ [10] that is responsible for producing heating energy under the influence of alternating current (AC) magnetic field [2]. The relaxation time constant

$\tau_m$ and magnetic loss tan δ have been calculated using the formula $\tau m = 1/2\pi f_{resonance}$ [5,6] and tan δ = M''/M' = $2\pi f_{resonance}$

$\tau m$ respectively [9-13]. Their calculated values are listed in the Table 2:
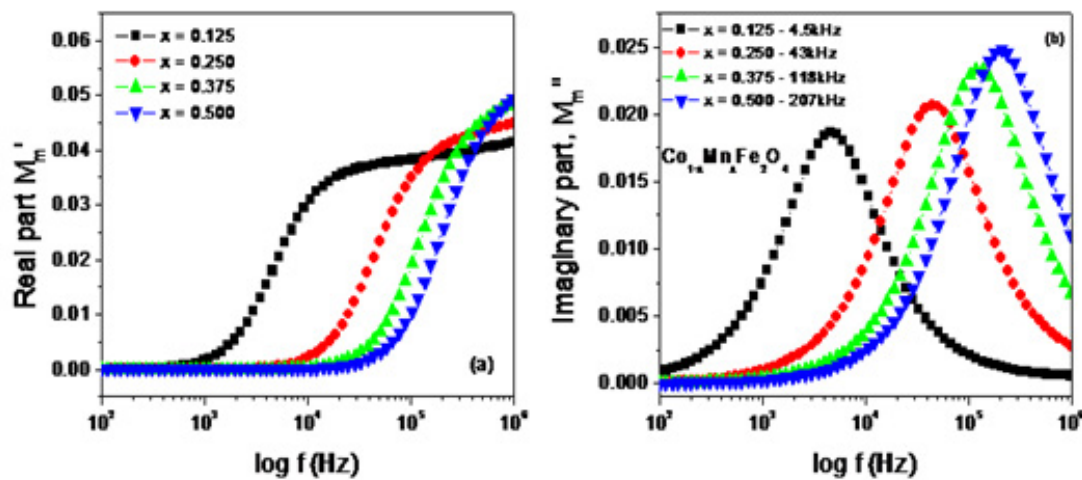


**Figure 4.** (a) spectrum of real part (M'm) (b) spectrum of imaginary part (M''m) at room temperature for examined samples.

**Table 2.** Resonance frequency, $f_{resonance}$, relaxation time constant, $\tau_m$ and loss tan δ of $Co_{1-x}Mn_xFe_{2x}O_4$

| Parameters | Mn(x) = 0.125 | Mn(x) = 0.25 | Mn(x) = 0.375 | Mn(x) = 0.5 |
|---|---|---|---|---|
| Spin resonance frequency, $f_{resonance}$ | 4.5 kHz | 43 kHz | 118 kHz | 207 kHz |
| Relaxation time, $\tau_m = 1/2\pi f_{resonance}$ | 37μs | 13μs | 1.35μs | 0.77μs |
| Magnetic loss tan δ = $2\pi f_{resonance}\,\tau_m$ | 0.166 | 0.559 | 0.1593 | 0.1594 |

From Table 2, both the resonance frequency, $f_{resonance}$ and relaxation time constant are found to be tunable $\tau m$ with the Mn content. The maximum magnetic loss tan δ is marked at the resonance frequency 43 kHz for the sample of Mn content (x) = 0.25 and minimum at 18kHz for the sample of Mn content (x) = 0.375 and implies the absorption of magnetic energy from the AC magnetic field that may dissipate in the form of heating energy as the magnetic relaxation loss. Besides, the magnitude of M''m at the corresponding resonance frequency $f_{resonance}$ is also marked to increase with increasing Mn content as seen from Figure-4(b) and infers the more absorption of magnetic energy from the magnetic field that in turn leading to a decrease the rotational resonance (spin rotation) in the material. Thus, the evolution of heating energy is also found to be tunable with the Mn content (x). Despite it, the specific absorption rate (SAR) is a measure of the rate at which energy is absorbed per unit mass by MNPs form the AC magnetic field. This SAR results from the relaxation process for MNPs.

In solid state, Neel relaxation process plays the dominant role to absorb the energy from the alternating magnetic field and is associated with the relaxation time constant, $\tau_m$ by the relation, $\tau_m = \tau 0 e^{KV/kT}$, where τ0 is the perfector, (usually τ0 ~ 1) K is the anisotropy constant, V is the volume of the particle, k is the Boltzmann constant and T is the absolute temperature [22,23]. Thus, the relaxation time constant, $\tau_m$ may optimize the required temperature in MNPs over the temperature range 40-47°C by tuning Mn content (x). This tunability of heating energy marks the sample suitable to be used in MIH for therapeutic treatment of tumor in the breast and beneath the skin through optimization and functionalizing the studied samples with biocompatible materials and therefore asserted as its novelty in this study.

Figure 5 displays single semicircle in their respective Nyquist plot that characterizes a single time constant of magnetic relaxation, in particular, spin relaxation across their grain boundaries. The dipolar orientation (wall resonance) and

spin rotation (resonance rotations) are found to occur (as indicated by the dotted red circle) and contributing to their magnetization as well permeability in the low-frequency range. However, the dipolar orientations (wall resonance) gradually damped with increasing applied frequency, and finally, only the spin rotations (resonance rotation) remains that play the role in increasing their permeability to a single asymptotic value. Hence, the frequency at which the domain wall motions completely ceased that symbolizes the onset of ferromagnetic resonance (FMR) resulting from the spin rotations only. This implies that ferrous and ferric ions dominate in the B site, which could be triggered by the migration of $Co^{2+}$ ions from the B to the A site and being replaced by $Mn^{2+}$ ions in the B site. As a result, permeability decreases with the increase of Mn content (x) due to their antiferromagnetic effect across the grain boundaries [17,24,25]. The energy loss associated with this FMR at the resonance frequency $f_{resonance}$ due to the imaginary part of magnetic modulus may be expressed by the relation $W = \pi J_p^2 M''$ joule, where Jp is the peak polarization during the magnetization process (usually $J_p \sim 1$ ) [26]. This magnetic loss may dissipate as the heat radiation energy by the MNPs of the sample and tunable with Mn content (x). This fact also confirms that the studied sample may be a suitable candidate to be used in hyperthermia therapy for the cancer treatment through optimizing to required temperature at around $47^0C$. The magnetic loss associated with FMR has been calculated and listed in the Table 3.
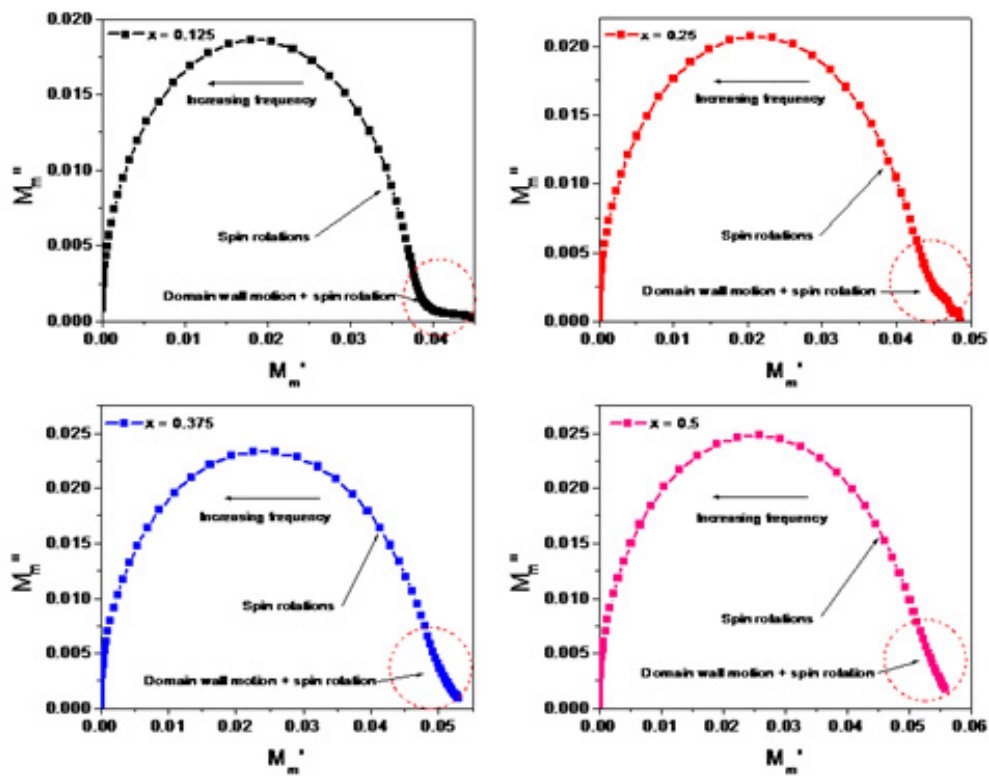


**Figure 5.** Nyquist plots at RT in the frequency range 100Hz – 10MHz for examined samples.

**Table 3.** Magnetic loss associated with FMR of $Co_{1-x}Mn_xFe_{2x}O_4$

| Parameters | Manganese content , Mn (x) | | | |
|---|---|---|---|---|
| | **0.125** | **0.25** | **0.375** | **0.5** |
| Magnetic loss associated with FMR, $W = \pi J_p^2 M''$ Joule | 0.0556 | 0.0659 | 0.076 | 0.0785 |

## ACHIEVABLE APPLICATIONS

a. The absorption of magnetic energy (magnetic loss associated with FMR) that ultimates to heating energy is found to be tunable by Mn content as shown in Table-3 (0.0556 – 0.0785J) that may facilitate the investigated sample to be used for hyperthermia therapeutic treatment of breast cancer and any other biological/medical related research after optimizing the required temperature and functionalizing it with the biocompatible materials.

b. Additionally, the constancy (non-responsiveness) of imaginary part of the complex permeability over the frequency band 1.5kHz – 1MHz implies the prospect of using this material in medical devices where low and constant temperature is required.

## CONCLUSION

The XRD profile shows the increasing trend of crystallite size (64.02nm – 67.17nm) with the manganese content that is correlated to the absorption of magnetic energy. The magnetic modulus extricates the local properties of defects on the complex permeability of the examined samples. As the real part of the complex magnetic modulus reaches to zero, it isolates the other stray results, such as air gap, etc. The raising trend in their real part of magnetic modulus with increasing applied frequency indicates that the wall relaxation and spin rotation are the only mechanism responsible for magnetization and also associated with the hysteresis and relaxation losses. The shifting of resonance peaks rightward with increasing manganese content implies the more absorption magnetic energy from the AC magnetic field to convert electromagnetic energy to heating energy. This absorption of magnetic energy that ultimates to heating energy is found to be tunable with the Mn content (Table 3).

## LIMITATION AND SUGGESTIONS OF THIS STUDY

### Limitations

1. The heating efficiency of MNPs was not determined to ascertain the applicability of the investigated samples in MIH by the magnetic relaxation loss, which is alleged here as the novelty of this study.

2. The probing of generated heat due to magnetic loss tan δ was not performed during experimentation because the objectives of this research were not aligned with the objective of this paper.

### Suggestions

1. An investigation is suggestive to probing generated heat due to magnetic relaxation loss.

2. Another investigation is suggestive to confirm its applicability in MIH by determining specific low power (SLP) and specific absorption rate (SAR) with these samples.

## ACKNOWLEDGMENTS

## DECLARATION OF INTEREST

We, the authors and our immediate family members, have no financial interests to declare. The authors declare no competing interests.

## DATA AVAILABILITY

No. Data will be made available on request.

## REFERENCES

1. Vassallo M, Martella D, Barrera G, Celegato F, Coïsson M, Ferrero R, et al. (2023). Improvement of Hyperthermia Properties of Iron Oxide Nanoparticles by Surface Coating. ACS Omega. 8(2):2143-2154.

2. Yu X, Yang R, Wu C, Liu B, Zhang W. (2022). The heating efficiency of magnetic nanoparticles under an alternating magnetic field. Sci Rep. 12(1):16055.

3. Garanina AS, Nikitin AA, Abakumova TO, Semkina AS, Prelovskaya AO, Naumenko VA, et al. (2021). Cobalt Ferrite Nanoparticles for Tumor Therapy: Effective Heating versus Possible Toxicity. Nanomaterials (Basel). 12(1):38.

4. Ahsan MZ, Islam MA, Khan FA. (2021). Tunability of ac conductivity in manganese doped cobalt ferrite nanoparticles. Results Phys. 2021:103782.

5. Ahsan MZ, Islam MA, Bally AA, Khan FA. (2020). Spectroscopic analysis for electric and magnetic properties of manganese doped cobalt nanoferrite. Results Phys. 2020:103172.

6. Ahsan MZ. (2020). Structural correlation and tunability of magnetic and electric properties of manganese doped cobalt ferrite nanoparticles. BUET (Dept of Physics) Thesis.

7. Annie Vinosha P, Manikandan A, Sherley Judith Ceicilia A, Dinesh A, Francisco Nirmala G, Christy Preetha A, et al. (2021). Review on recent advances of zinc substituted cobalt ferrite nanoparticles: Synthesis characterization and diverse applications. Ceramics International. 47(8):10512-10535.

8. Yu S, Zhang H, Zhang S, Zhong M, Fan H. (2021). Ferrite Nanoparticles-Based Reactive Oxygen Species-Mediated Cancer Therapy. Front Chem. 9:651053.

9. Ahsan MZ, Kamal MM, Rakhi SS, Tanha SN, Hasan GI. (2023). Electric modulus of manganese doped cobalt ferrite nanoparticles. Results in Physics. 50:106593.

10. Shubitidze F, Kekalo K, Stigliano R, Baker I. (2015). Magnetic nanoparticles with high specific absorption rate of electromagnetic energy at low field strength for hyperthermia therapy. J Appl Phys. 117(9):094302.

11. Salih SJ, Mahmood WM. (2023). Review on magnetic spinel ferrite ($MFe_2O_4$) nanoparticles: From synthesis to application. Heliyon. 9(6):e16601.

12. Shahbahrami B, Rabiee SM, Shidpoor R. (2020). An Overview of Cobalt Ferrite Core-Shell Nanoparticles for Magnetic Hyperthermia Applications. Advanced Ceramics Progress, ACER.

13. Kerroum MAA, Iacovita C, Baaziz W, Ihiawakrim D, Rogez G, Benaissa M, et al. (2020). Quantitative Analysis of the Specific Absorption Rate Dependence on the Magnetic Field Strength in $Zn_xFe_{3-x}O_4$ Nanoparticles. Int J Mol Sci. 21(20):7775.

14. Ahsan MZ, Khan FA, Islam MA. (2019). Frequency and temperature dependent intrinsic electric properties of manganese doped cobalt ferrite nanoparticles. Results Phys. 14:102484.

15. Ahsan MZ, Khan FA, Islam MA. (2019). Frequency and temperature dependent dielectric and magnetic properties of Manganese doped Cobalt ferrite nanoparticles. Journal of Electronic Materials. 48:7721-7729.

16. Yu X, Yang R, Wu C, Zhang W. (2020). Effect of chromium ion substitution of ZnCo ferrites on magnetic induction heating. J Alloys Compd. 830:154724.

17. Ahsan MZ, Khan FA. (2018). Structural and electrical properties of manganese doped cobalt ferrite nanoparticles. Mater Sci Nanotechnol. 2(2):1-9.

18. Purnama B, Wijayanta AT, Suharyana. (2019). Effect of calcination temperature on structural and magnetic properties in cobalt ferrite nanoparticles. J King Saud Univ–Sci. 31(4):956-960.

19. Jian Chin C, Wen-Cheng C, Yin-Chun T, Chi-Jen S. (2010). Effect of calcination temperature on the crystallite growth of cerium oxide nanopowders prepared by the co-precipitation process. J Alloys Compd. 496(1-2):364-369.

20. Tapdiya S, Shrivastava AK, Singh S. (2017). Effect of Mn substitution on structural and magnetic properties of cobalt ferrite. Advanced Materials Proceedings. 2(9):547-551.

21. Jyotsnendu G, Pallab P, Sriharsha T, Bahadur D. (2005). Preparation and investigation of potentiality of different soft ferrites for hyperthermia applications. Journal of Appl Phys. 97(10):10Q916.

22. Samrot AV, Sahithya CS, Selvarani JA, Purayil SK, Ponnaiah P. (2021). A review on synthesis, characterization and potential biological applications of superparamagnetic iron oxide nanoparticles. Current Research in Green and Sustainable Chemistry. 4:100042.

23. Khan FA. (2017). Study of structural and magnetic properties of manganese doped cobalt ferrite nanoparticles for high frequency and sensor application. J Material Sci Eng (Suppl).

24. Pasquale M, Fiorillo F, Coisson M, Beatrice C. (2008). Magnetic permeability, loses and Ferromagnetic Resonance in Ferrite under magnetic field bias from dc to the microwave regime 2008 Conference on Precision Electromagnetic Measurements Digest, Broomfield, CO, USA.

25. Chang D, Lim M, Goos JACM, Qiao R, Ng YY, Mansfeld FM, et al. (2018). Biologically Targeted Magnetic Hyperthermia: Potential and Limitations. Front Pharmacol. 9:831.

26. Dunn AE, Dunn DJ, Lim M, Boyer C, Thanh NTK. (2013). Recent developments in the design of nanomaterials for photothermal and magnetic hyperthermia induced controllable drug delivery. Nanoscience. 2:225-254.